GNAS mutation inhibits growth and induces phosphodiesterase 4D expression in colorectal cancer cell lines

Nummela, Pirjo; Zafar, Sadia; Veikkolainen, Erika; Ukkola, Iiris; Cinella, Vincenzo; Ayo, Abiodun; Asghar, Muhammad Yasir; Välimäki, Niko; Törnquist, Kid; Karhu, Auli; Laakkonen, Pirjo; Aaltonen, Lauri A.; Ristimäki, Ari

Published in:
International Journal of Cancer

DOI:
10.1002/ijc.34865

Published: 01/06/2024

Document Version
Final published version

Document License
CC BY

Received: 17 May 2023 | Revised: 31 December 2023 | Accepted: 10 January 2024

DOI: 10.1002/ijc.34865

RESEARCH ARTICLE

Molecular Cancer Biology

IJC INTERNATIONAL JOURNAL of CANCER

GNAS mutation inhibits growth and induces phosphodiesterase 4D expression in colorectal cancer cell lines

Pirjo Nummela[1,2] | Sadia Zafar[1,2] | Erika Veikkolainen[1,2] | Iiris Ukkola[1,2] | Vincenzo Cinella[1,2] | Abiodun Ayo[3] | Muhammad Yasir Asghar[4,5] | Niko Välimäki[1,6] | Kid Törnquist[5,7] | Auli Karhu[1,6] | Pirjo Laakkonen[3] | Lauri A. Aaltonen[1,6] | Ari Ristimäki[1,2]

[1]Applied Tumor Genomics Research Program, Research Programs Unit, University of Helsinki, Helsinki, Finland

[2]Department of Pathology, HUSLAB, HUS Diagnostic Center, University of Helsinki and Helsinki University Hospital, Helsinki, Finland

[3]Translational Cancer Medicine Research Program, Research Programs Unit, University of Helsinki, Helsinki, Finland

[4]Cell and Tissue Dynamics Research Program, Institute of Biotechnology, HiLife, University of Helsinki, Helsinki, Finland

[5]Minerva Foundation Institute for Medical Research, Helsinki, Finland

[6]Department of Medical and Clinical Genetics, University of Helsinki, Helsinki, Finland

[7]Faculty of Science and Engineering, Cell Biology, Åbo Akademi University, Turku, Finland

Correspondence
Pirjo Nummela, Research Programs Unit, University of Helsinki, P.O. Box 63, FI-00014 Helsinki, Finland.
Email: pirjo.nummela@helsinki.fi

Present address
Vincenzo Cinella, Dana-Farber Cancer Institute, Boston, Massachusetts, USA.

Funding information
Syöpäsäätiö; Medicinska Understödsföreningen Liv och Hälsa; Finska Läkaresällskapet; Helsingin Yliopisto; Helsingin ja Uudenmaan Sairaanhoitopiiri; Sigrid Juséliuksen Säätiö

Abstract

Approximately 5% of colorectal cancers (CRCs) have a gain-of-function mutation in the *GNAS* gene, which leads to the activation of cAMP-dependent signaling pathways and associates with poor prognosis. We investigated the effect of an activating *GNAS* mutation in CRC cell lines on gene expression and cell proliferation in vitro, and tumor growth in vivo. *GNAS*-mutated (GNASmt) HCT116 cells showed stimulated synthesis of cAMP as compared to parental (Par) cells. The most upregulated gene in the GNASmt cells was cAMP-hydrolyzing *phosphodiesterase 4D* (*PDE4D*) as detected by RNA sequencing. To further validate our finding, we analyzed *PDE4D* expression in a set of human CRC tumors (n = 35) and demonstrated overexpression in *GNAS* mutant CRC tumors as compared to *GNAS* wild-type tumors. The GNASmt HCT116 cells proliferated more slowly than the Par cells. PDE4 inhibitor Ro 20-1724 and PDE4D subtype selective inhibitor GEBR-7b further suppressed the proliferation of GNASmt cells without an effect on Par cells. The growth inhibitory effect of these inhibitors was also seen in the intrinsically *GNAS*-mutated SK-CO-1 CRC cell line having high levels of cAMP synthesis and *PDE4D* expression. In vivo, GNASmt HCT116 cells formed smaller tumors than the Par cells in nude mice. In conclusion, our findings demonstrate that *GNAS* mutation results in the growth suppression of CRC cells. Moreover, the *GNAS* mutation-induced overexpression of PDE4D provides a potential avenue to impede the proliferation of CRC cells through the use of PDE4 inhibitors.

KEYWORDS
cAMP, colorectal cancer, GNAS, PDE4, phosphodiesterase

What's new?

An activating mutation in the *GNAS* gene is associated with worse prognosis in colorectal cancer (CRC). Here, the authors investigate the molecular and functional effects of these mutations. In

Pirjo Nummela and Sadia Zafar contributed equally to this study.

cultured CRC cells, they showed that *GNAS* mutations induced cells to make more cAMP and cAMP-hydrolyzing enzymes. Inhibiting these enzymes suppressed CRC cell proliferation, suggesting that these inhibitors could potentially be used to slow the growth of CRC tumors with *GNAS* mutations.

1 | INTRODUCTION

The intracellular level of cyclic adenosine monophosphate (cAMP) is tightly controlled by the balance of production by adenylyl cyclase (AC) and degradation by cyclic nucleotide phosphodiesterase (PDE).[1] The upstream signal that stimulates the synthesis of cAMP is largely provided by the stimulatory α subunit ($G\alpha_s$) of heterotrimeric guanine nucleotide-binding protein (G protein). Activated $G\alpha_s$ transduces signals from G protein-coupled receptors (GPCRs) to AC, which becomes activated and produces cAMP. $G\alpha_s$ subunit is encoded by the *GNAS* (guanine nucleotide binding protein, alpha stimulating) gene, and activating mutations of this gene lead to reduced intrinsic GTPase activity of the $G\alpha_s$, rendering it and cAMP-dependent signaling pathways to become activated.[1,2] In addition to the major effector protein kinase A (PKA), cAMP is capable of activating other effectors, including exchange protein directly activated by cAMP (EPAC), cyclic nucleotide-gated ion channels and Popeye domain containing proteins.[1,3]

There is a striking enrichment of $G\alpha_s$-pathway activation in cancers of the gastrointestinal tract, and over half of the colorectal cancers (CRC) have aberrantly turned on this pathway by activation of GPCRs or by gene mutations and rearrangements.[1,2] The occurrence of *GNAS* mutations in CRC is 4.8% according to a recent meta-analysis, most of them being either R201C or R201H, which associate with poor prognosis and resistance to oncological treatments.[4,5] However, the role of *GNAS* mutations in gastrointestinal carcinogenesis is somewhat contradictory, since they are predominantly found in precursor lesions and are thought to be important only in the initiation phase of carcinogenesis.[1] In addition to activation of $G\alpha_s$, it is intriguing that PDE dysregulation also occurs in CRC.[1,6]

PDEs hydrolyze the phosphodiester bond of cAMP and/or cGMP, yielding non-cyclic nucleotides unable to transmit downstream signaling.[7] Altogether 21 human *PDE* genes are known, and PDE enzymes are subdivided into 11 families (PDE1-11) based on sequence homology, enzymatic properties and sensitivity to inhibitors. Each family contains several transcript variants with unique tissue and subcellular distribution, regulation of expression and post-translational modification.[8] Expression of two cAMP-specific PDE subtypes, PDE4B and PDE4D, has been shown to be elevated in CRC and modulate the growth and survival of CRC cells.[6] While there exist no pharmacological inhibitors for $G\alpha_s$, PDE inhibitors have been investigated as potential therapeutic agents in various diseases. Some of these inhibitors have already been approved for the treatment of cardiovascular diseases (PDE3 inhibitors), pulmonary hypertension and erectile dysfunction (PDE5 inhibitors) and inflammatory conditions (PDE4 inhibitors).[9] There is an increasing interest in PDE inhibitors as a therapeutic option for malignant diseases.[1,6,9] Interestingly, PDE4D overexpression has been previously reported in several solid tumor types, including colon, gastric, pancreatic, hepatocellular, prostatic, endometrial and ovarian carcinoma, as well as in melanoma.[10–14]

In this study, we investigated the effect of an activating *GNAS* mutation in CRC cell lines on gene expression, cell proliferation in vitro and tumor growth in vivo. We show that *GNAS* mutation-induced effects in CRC cells are counteracted by overexpression of PDE4D, which can be reversed by using PDE4 inhibitors.

2 | MATERIALS AND METHODS

2.1 | Cell Culture

Parental (Par) colon cancer cell line HCT116 (RRID:CVCL_0291) and its CRISPR/Cas9 edited descendant bearing activating *GNAS* R201C/+ mutation (RRID:CVCL_LD67; GNASmt; Horizon Discovery Ltd., Cambridge, UK) were cultured in RPMI 1640 medium supplemented with Penicillin-Streptomycin, GlutaMAX Supplement and 10% Fetal Bovine Serum (Thermo Fisher Scientific, Waltham, MA). SK-CO-1 CRC cell line (RRID:CVCL_0626) was purchased from ATCC (Manassas, VA) and grown in EMEM medium (Merck, Burlington, MA) supplemented with the above-mentioned additives and 1 mM sodium pyruvate (Merck). All cell lines were authenticated using short tandem repeat (STR) profiling within the last 3 years by FIMM Genomics (Helsinki Institute of Life Science HiLIFE and Biocenter Finland, University of Helsinki, Helsinki, Finland). All experiments were performed with mycoplasma-free cells.

2.2 | Chemicals

Chemicals including their catalog numbers are as follows: DMSO (D2650; Merck), ESI-09 (4773; Tocris Bioscience/Bio-Techne Ltd., Minneapolis, MN), forskolin (FSK) (F3917; Merck), GEBR-7b (524748; Calbiochem/Merck), H89 (B1427; Merck), IBMX (I7018; Merck), Ro 20-1724 (B8279; Merck), staurosporine (HY-15141; MedChemExpress, Monmouth Junction, NJ) and 666-15 (HY-101120; MedChemExpress).

2.3 | siRNA transfection

To knock down *GNAS* expression, HCT116 and SK-CO-1 cells were transfected with siRNAs utilizing Lipofectamine™ RNAiMAX transfection reagent (Thermo Fisher Scientific) according to the manufacturer's protocol, using 10 nM siRNA concentration, OPTI-MEM I reduced serum medium and 48 or 72 h transfection time. The siRNAs used for *GNAS* knockdown were s526399 (siRNA #2) and s5891

(siRNA #4), while Silencer Select GAPDH Positive control siRNA and Silencer Select Negative control #2 siRNA were used as controls. All experiments were repeated at least three times with two or three biological replicates.

2.4 | cAMP assay

Basal cAMP synthesis/accumulation rates of the cell lines were investigated using cAMP-Glo Max Assay (Promega, Madison, WI) according to the kit instructors. For the assay, 8000 cells were seeded into Corning BioCoat poly-D-lysine-treated 96-well plates the previous day, and at the start of the assay the cells were incubated for 2 to 3 h in Complete Induction Buffer (containing 500 μM pan-PDE inhibitor IBMX and 100 μM PDE4 inhibitor Ro 20-1724 to enable cAMP accumulation). The experiments were repeated at least three times with four to six replicates.

2.5 | RNA-Seq analysis

Total RNA was extracted from cell pellets using NucleoSpin RNA kit (Macherey-Nagel GmbH & Co. KG, Düren, Germany) according to the instructions. RNA quality and quantity were measured with NanoDrop spectrophotometer (Thermo Fischer Scientific). The quality of total RNA was further verified with Agilent 2200 TapeStation and RNA ScreenTapes (Agilent Technologies, Santa Clara, CA). RNA sequencing (RNA-Seq) service was performed by the Biomedicum Functional Genomics Unit (HiLIFE and Biocenter Finland, University of Helsinki, Helsinki, Finland) using mRNA purification with polyA-binding beads, NEBNext Ultra II Directional RNA Library Prep kit (New England BioLabs, Ipswich, MA) and single-end sequencing (read length 75 bp) using Illumina NextSeq sequencer (Illumina, San Diego, CA) with a High Output run. Four biological replicates were analyzed. The data quality was first analyzed with FastQ and summarized with MultiQC, light quality trimming was done with Trimmomatic and the sample reads were aligned against the human GRCh38.p12 reference genome with STAR, with mapping quality assessment done with Qualimap. To quantify the aligned reads, featureCounts was used. Finally, differential expression statistics were calculated with DESeq2 and basic gene annotation was obtained using Ensembl release 97. The sequencing coverage and quality statistics for each sample are summarized in Table S1.

2.6 | Quantitative polymerase chain reaction

The cDNA synthesis was performed for 1 μg of total RNA by using GoScript Reverse Transcriptase (Promega) according to the instructions, using Oligo(dT)$_{15}$ primers and 3 mM $MgCl_2$ (Promega). The quantitative polymerase chain reaction (qPCR) analyses were performed as previously published[15] utilizing TaqMan® Gene Expression Assays for *RPL13A* (Hs04194366_g1, VIC-MGB, used as an endogenous reference gene), *GAPDH* (Hs02786624-g1, FAM-MGB), *GNAS* (Hs00255603_m1, FAM-MGB), *PDE4B* (Hs00277080_m1, FAM-MGB) and *PDE4D* (Hs01579625_m1, FAM-MGB) (Thermo Fisher Scientific), and AB 7500 Fast Real-Time PCR System (Applied Biosystems/Thermo Fisher Scientific). All experiments were repeated at least three times with two or three biological replicates and three technical replicates.

2.7 | Reverse transcription-PCR

PDE4D transcript variants expressed in the studied cell lines were analyzed using reverse transcription (RT)-PCR. For PCR, 1/10 vol of cDNA synthesized as above, dNTP mix, DreamTaq DNA polymerase (Thermo Fischer Scientific) and isoform-specific primers (Eurofins Genomics, Ebersberg, Germany) were mixed and amplified using standard PCR protocol. Details of the primers and PCR conditions are presented in Table S2. Primer sequences for *PDE4D7* were from Wang et al[16] and for other isoforms from Lin et al.[11] The PCR products were finally resolved in 2% agarose gel, using Midori Green Advance DNA Stain (Nippon Genetics Europe GmbH, Düren, Germany) for visualization. A549 total RNA and human brain total RNA (Takara Bio Europe, Saint-Germain-en-Laye, France) were used as positive controls, and *actin beta* (*ACTB*) primers were used as a loading control.

2.8 | Western blotting

Sample preparation and Western blot analysis was performed as described previously.[15] The cells were lysed with RIPA buffer containing protease inhibitor cocktail (Roche, Basel, Switzerland) and protein concentrations were quantitated using BCA Protein Assay Kit (Pierce/Thermo Scientific). For Western blotting, samples containing 50 μg of total proteins were then separated by 4% to 15% SDS-PAGE gels (4561084; Bio-Rad Laboratories AB, Hercules, CA) and transferred onto nitrocellulose membranes using Trans-Blot Turbo Transfer System (Bio-Rad Laboratories AB). The membranes were blocked with 3% BSA in Tris-buffered saline +0.1% NP40 overnight at +4°C and then immunoblotted using PDE4D rabbit monoclonal antibody (MA5-38426; ThermoFisher Scientific), HRP-conjugated anti-rabbit secondary antibody (P0448; DAKO/Agilent, Santa Clara, CA) and SuperSignal West Pico PLUS Chemiluminescent Substrate (Thermo Scientific). Equal loading of the samples was confirmed with mouse anti-α-tubulin antibody (ab7291; Abcam, Cambridge, UK) and HRP-conjugated anti-mouse secondary antibody (P0260; DAKO/Agilent).

2.9 | Cell viability assay

For analysis of cell proliferation, 1000 HCT116 cells or 6000 SK-CO-1 cells were seeded into black flat-bottom 96-well plates (Fisher Scientific, Loughborough, UK), and PDE4 inhibitors (PDE4 selective Ro 20-1724 or PDE4D selective GEBR-7b), FSK or DMSO control (Ctrl), were added the next day. After preliminary titrations, the final

concentrations used were 10 μM for Ro 20-1724 and FSK, and 10 μg/mL for GEBR-7b, and DMSO was analogously used at 0.05%. Relative cell numbers were calculated from fluorescence measured at 0, 48 and 72 h after the addition of the inhibitors by using the CellTiter-Blue Cell Viability Assay (Promega). The redox dye resazurin-containing reagent was incubated for 1 h before measurement of fluorescence (Ex 544 nm, Em 590 nm) by FLUOstar Omega plate reader (BMG Labtech, Ortenberg, Germany). All the experiments were repeated at least three times with four to six replicates.

2.10 | Thymidine incorporation assay

As a second method to inspect cell proliferation, a ^{3}H-thymidine incorporation assay was used. Briefly, 50,000 cells were seeded into six-well plates and allowed to grow overnight. The next day, the medium was changed to fresh one containing DMSO (0.05%; Ctrl), GEBR-7b (10 μg/mL), Ro 20-1724 (10 μM) or FSK (10 μM) and the cells were allowed to proliferate for 24, 48 or 72 h. Four hours before each time-point, 0.4 μCi/mL ^{3}H-thymidine (PerkinElmer, Waltham, MA) was added. At each time point, the cells were washed three times with PBS and incubated for 10 min with 5% trichloroacetic acid and then 10 min with 0.1 M NaOH. Finally, the samples were transferred into scintillation tubes, high sample load scintillation cocktail Optiphase Hisafe 3 (PerkinElmer) was added, and radioactivity was measured using Wallac 1414 liquid scintillation counter (PerkinElmer). All experiments were repeated at least three times with three biological replicates.

2.11 | Apoptosis assay

For analysis of apoptosis, Caspase-Glo 3/7 Assay (Promega) was performed according to the manufacturer's instructions. For the assay, 7500 HCT116 or 10000 SK-CO-1 cells were seeded into white clear bottom 96-well plates (3610; Corning), and PDE4 inhibitors, FSK or DMSO Ctrl were added the next day. The concentrations used were the same as above. Staurosporine (1 or 5 μM) was used as a positive control. After the addition of the inhibitors, the cells were incubated for 24 h. The Caspase-Glo 3/7 Reagent was added and incubated for 1 h before measuring the luminescence with FLUOstar Omega plate reader (BMG Labtech). All the experiments were repeated at least three times with three to four replicates.

2.12 | In vivo xenograft assays

For animal experiments, 4-weeks old female NMRI-Foxn1 nude mice were purchased from Janvier laboratories (www.janvier-labs.com) and maintained in ventilated caging rack system under a pathogen free environment in the University of Helsinki Biomedicum Animal Facility, in accordance with the ethical guidelines of the provincial government of Finland. For in vivo tumor growth assay, 1×10^{6} HCT116 Par and GNASmt cells in 1:1 diluted Matrigel were implanted subcutaneously into the flanks of the immunodeficient mice (one flank per animal, eight mice per study group). Starting from day seven, the tumor sizes were measured twice per week using a digital caliper 0.150 mm (Cocraft stainless hardened) and all animals were sacrificed when the largest tumor reached ethical limits. The weight of the mice was measured twice a week. Tumor data were normalized to day seven, which was set as 100%.

2.13 | Analysis of *PDE4D* expression in CRC tumors stratified by *GNAS* mutation status

PDE4D mRNA expression was analyzed from an existing whole genome sequencing (WGS) and RNA-Seq data of CRC material ($n = 34$) described in Cajuso et al.[17] Further, one extra sample analyzed in similar way was included. WGS mutation statuses were compiled with BasePlayer.[18] Salmon (version 0.12.0; quant mode with --validateMappings) was used to map raw sequences onto the human transcriptome (Ensembl release 79). Gene-level quantification and differential gene expression (DE) analysis were done with DESeq2 (v1.18.1) using default options. Variance stabilizing transformation was used to estimate logarithmic-scale values for gene expression visualization. For DE, we report fold-change (FC) and *P*-value (DESeq2 Wald test).

2.14 | Immunohistochemistry

The mouse xenograft tumors were cut into two halves, fixed for 24 h with formalin, transferred into 70% ethanol for at least 1 h and embedded in paraffin using Tissue-Tek TEC Embedding System (Sakura Finetek, Tokyo, Japan). HE staining was performed with a routine protocol. For analysis of cell proliferation (Ki67) and apoptosis (cleaved caspase 3), the sections were deparaffinized and rehydrated, subjected to heat-induced epitope retrieval (HIER) in 10 mM Tris, 1 mM EDTA (pH 9.0) and incubated 1 h at RT with the primary antibodies (rabbit anti-Ki67, ab92742, Abcam or rabbit anti-Cleaved Caspase 3, #9661, Cell Signaling Technology, Danvers, MA) using dilutions 1:500 and 1:200, respectively. For detection, BrightVision goat anti-rabbit HRP (DPVR-110HRP, Immunologic, Duiven, the Netherlands) was incubated for 30 min at RT and BrightDAB (BS04-110; Immunologic) for 8 min at RT. The percentages of immunopositive cells were determined from six high-power fields (×400) of the vital tumor areas, counting positive nuclei for Ki67 staining and positive cytoplasm for cleaved caspase 3 staining.

For analysis of PDE4D protein expression on human CRC tumors, 30 formalin-fixed, paraffin-embedded diagnostic tissue specimens from the CRC set described above were available (all four *GNAS* mutant cases were included). Exactly 4-μm sections were cut with Leica SM2000R microtome (Leica Microsystems GmbH, Wetzlar, Germany), deparaffinized and rehydrated with Tissue-Tek DRS (Sakura Finetek) and subjected to HIER with PT Link (DAKO/Agilent) using EnVision FLEX Target Retrieval Solution Low pH (pH 6.1; DAKO/Agilent). The immunostaining was performed with EnVision FLEX kit (DAKO/Agilent), according to the instructions, using Lab Vision Autostainer 480 (Thermo Fisher Scientific). Two distinct primary rabbit anti-PDE4D antibodies

were used (12918-1-AP, 1:400, Proteintech, Rosemont, IL or LS-B15091-100, 1:50, LSBio, Shirley, MA) and incubated for 1 h at RT. For detection, DAB was incubated for 10 min. The immunostainings of the carcinoma areas were scored as weak (+), intermediate (++) or strong (+++). Similar results were obtained with both antibodies and results are shown for the 12918-1-AP antibody.

2.15 | Statistical analyses

All the graphs show results as mean ± SEM. Statistical significance ($P < .05$) for the differential gene expression by RNA-Seq was evaluated by Benjamini-Hochberg adjusted *P*-values using R. The difference in the in vitro assays was evaluated by the two-tailed Mann-Whitney *U* test using Prism 9 (GraphPad Software, San Diego, CA). For the in vivo experiment, Sidak's multiple comparison tests were analyzed with 2-way ANOVA using Prism 9 (GraphPad Software).

3 | RESULTS

3.1 | *GNAS* mutation stimulates cAMP synthesis in HCT116 CRC cells

GNASmt HCT116 cells showed increased cAMP synthesis as compared to Par cells (Figure 1A). Knock down of *GNAS* expression by *GNAS* siRNAs blocked the *GNAS* mutation-induced synthesis of cAMP, without any effect on the Par cells (Figure 1B). The effect of *GNAS* siRNAs on *GNAS* mRNA expression is shown in Figure S1A.

3.2 | *GNAS*-mutated HCT116 cells show striking upregulation of *PDE4D* expression

GNASmt HCT116 cells showed altogether 159 significantly upregulated genes and 130 downregulated genes when compared to the Par cells as analyzed by RNA-Seq and using FC 2.0 as a cutoff (Table S3). The most highly induced gene was *PDE4D* (FC > 700, $P < .00001$), which was clearly the most upregulated of any cAMP-cleaving PDEs (Table 1). Although *PDE4B* expression was relatively high in the Par cells, it was only modestly (1.5-fold) induced in the GNASmt cells (Table 1). The prominent upregulation of *PDE4D*, as well as the moderate increase in *PDE4B*, was verified with qPCR (Figure 2A,B). The strong induction of *PDE4D* expression in the GNASmt cells was effectively downregulated by *GNAS* siRNAs (Figure 2C), while they showed no effect or only a modest effect on *PDE4B* expression (Figure 2D). Among the transcript variants of *PDE4D*, induction seemed to specifically target the short and supershort variants *PDE4D1*, *PDE4D2* and *PDE4D6* (Figure S2A). This was supported by protein-level data obtained by using Western blotting (Figure S2B). Related to the potential downstream signaling mediating

TABLE 1 Expression of cAMP-hydrolyzing phosphodiesterases in parental and *GNAS*-mutated HCT116 cells as detected by RNA sequencing.

	Expression (mean ± SD)			
Gene	Par	GNASmt	FC	*P*-value[a]
PDE1A[b]	6 ± 2	4 ± 3	−1.5	
PDE1B[b]	8 ± 4	5 ± 3	−1.5	.447
PDE1C[b]	1 ± 1	1 ± 1	2.8	
PDE2A[b]	289 ± 14	288 ± 23	1.0	.979
PDE3A[b]	13 ± 5	12 ± 5	−1.1	.779
PDE3B[b]	1306 ± 16	1020 ± 14	−1.3	<.00001
PDE4A	2980 ± 97	2822 ± 52	−1.1	.040
PDE4B	6755 ± 85	10,241 ± 30	1.5	<.00001
PDE4C	3 ± 2	4 ± 2	1.4	
PDE4D	6 ± 3	4500 ± 109	722.7	<.00001
PDE7A	1349 ± 30	1337 ± 42	1.0	.850
PDE7B	35 ± 4	42 ± 12	1.2	.427
PDE8A	2762 ± 53	3187 ± 44	1.2	<.00001
PDE8B	4 ± 0	6 ± 1	1.5	
PDE10A[b]	22 ± 3	54 ± 8	2.5	<.00001
PDE11A[b]	67 ± 8	48 ± 4	−1.4	.037

Abbreviations: FC, Fold Change; mt, mutated; Par, parental; PDE, phosphodiesterase.
[a]Benjamini-Hochberg adjusted.
[b]Cleaving both cAMP and cGMP.

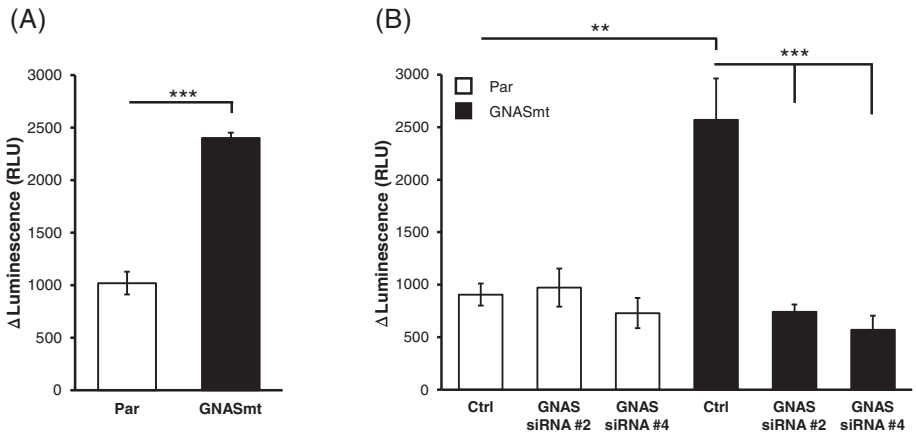

FIGURE 1 Effect of *GNAS* R201C mutation on cAMP synthesis in HCT116 colorectal cancer cells as analyzed by cAMP Glo Max assay. (A) cAMP accumulation in parental (Par) and GNAS-mutated (GNASmt) cells. (B) cAMP accumulation in Par and GNASmt cells after treatment with *GNAS* siRNAs. Scrambled siRNA was used as a control (Ctrl). The values are means ± SEM from two independent experiments (n = 8). ** $P < .01$, *** $P < .001$.

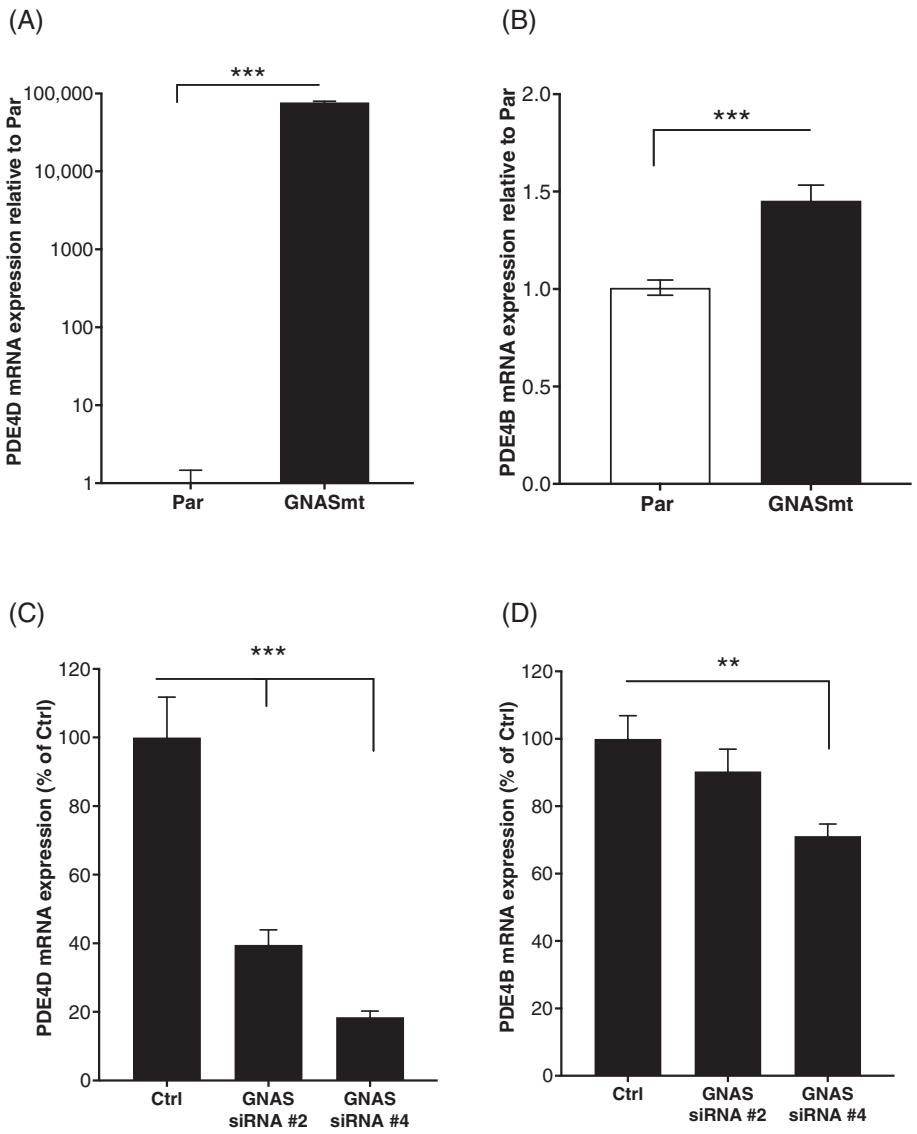

FIGURE 2 Effect of *GNAS* mutation on expression of *PDE4D* and *PDE4B* transcripts in HCT116 cells as analyzed by qPCR. (A) *PDE4D* expression in Par and GNASmt cells. (B) *PDE4B* expression in Par and GNASmt cells. (C) *PDE4D* expression in GNASmt cells after treatment with *GNAS* siRNAs. (D) *PDE4B* expression in GNASmt cells after treatment with *GNAS* siRNAs. Scrambled siRNA was used as a control (Ctrl). The values are means ± SEM from three independent experiments (n = 9). ** $P < .01$, *** $P < .001$.

the effect of cAMP, PKA and cAMP response element-binding protein (CREB) inhibitors effectively downregulated *PDE4D* transcript expression (41% and 53% inhibition, respectively), whereas EPAC inhibitor had a minor effect (22% inhibition) (Figure S3). Based on RNA-Seq data, PKA subunits also showed higher expression levels in GNASmt cells than EPACs, *PRKAC*s and *PRKAR*s giving thousands of reads (*PRKACB* mean value being 11,000 and *PRKAR1A* mean value 15,000), whereas the values for both *RAPGEF3* and *RAPGEF4* (coding for EPAC1 and EPAC2, respectively) were below 100 (Table S3 and data not shown).

3.3 | PDE4 inhibition suppresses the proliferation of GNASmt HCT116 cells

GNASmt cells proliferated more slowly than the Par cells (28% inhibition as compared to the Par cells at 72 h, $P < .001$) as analyzed by metabolic activity-dependent cell viability assay (Figure 3A). PDE4 selective inhibitor Ro 20-1724 or PDE4D subtype selective inhibitor GEBR-7b further inhibited the proliferation of GNASmt cells (42% and 45% inhibition, respectively, as compared to the Par cells at 72 h, *P*-values <0.001), without an effect on Par cells (Figure 3A). FSK showed a similar effect on the proliferation of GNASmt cells (46% inhibition as compared to the Par cells at 72 h, $P < .001$; Figure 3A). The proliferation impairment was further verified with thymidine incorporation assay. In this assay, GNASmt cells showed a 22% inhibition as compared to the Par cells, and PDE4 inhibitors showed a 40% to 41% suppression as compared to the Par cells in a 72 h experiment (Figure 3B). FSK inhibited thymidine incorporation in both Par and GNASmt cells by 19% and 60%, respectively, as compared to the Par Ctrl cells at the 72 h time point (Figure 3B). Our results suggest that cell growth is here the key target of *GNAS* mutation, since it did not induce apoptosis when compared to the Par cells in caspase 3/7 activity assay (Figure S4A). Furthermore, Ro 20-1724 did not induce apoptosis in Par or GNASmt cells, and GEBR-7b and FSK induced only a slight increase (1.1- and 1.2-fold, respectively) in GNASmt cells without any effect on the Par cells. As a positive control, 5 μM staurosporine induced over 3-fold caspase activation in both Par and GNASmt cells (data not shown).

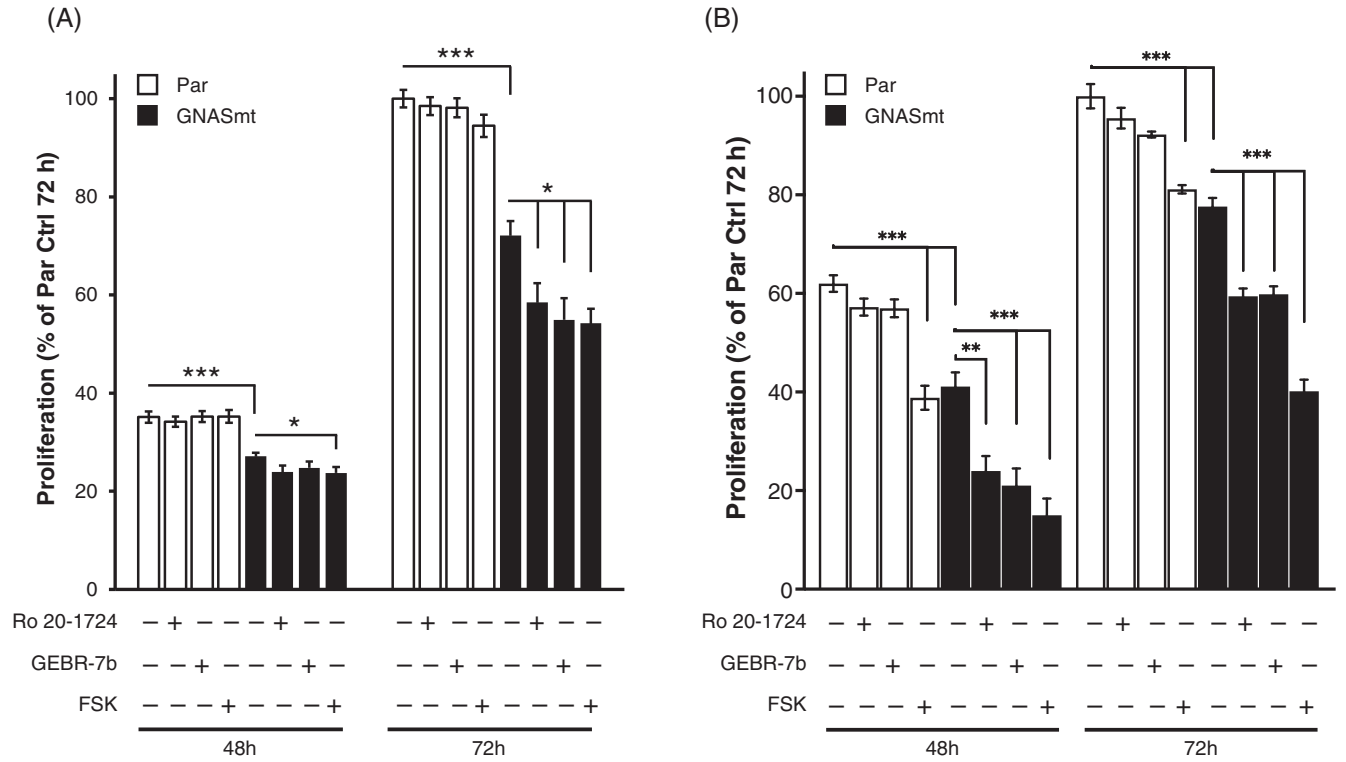

FIGURE 3 Effect of *GNAS* mutation and PDE4 inhibitors on proliferation of HCT116 cells. (A) Proliferation of Par and GNASmt cells with and without PDE4 inhibitors (PDE4 selective inhibitor Ro 20-1724, 10 μM and PDE4D selective inhibitor GEBR-7b, 10 μg/mL) or forskolin (FSK, 10 μM) as analyzed with CellTiter Blue Cell Viability Assay. (B) Thymidine incorporation assay of Par and GNASmt cells with and without the PDE4 inhibitors or FSK. The values are means ± SEM from three independent experiments (n = 12 in A, n = 9 in B). * $P < .05$, ** $P < .01$, *** $P < .001$.

FIGURE 4 Tumor growth of HCT116 cells in vivo, and expression of *PDE4D* transcript in human colorectal cancer (CRC) specimens. (A) Growth curves of Par and GNASmt tumors in nude mice. The data are presented as mean ± SEM (* $P < .05$; eight mice in both groups). (B) Expression of *PDE4D* mRNA (ENSG00000113448) in human CRC samples (n = 35) with or without *GNAS* mutations. The horizontal line denotes the median among *GNAS* wild-type tumors; the first and third quartiles are marked with dashed lines.

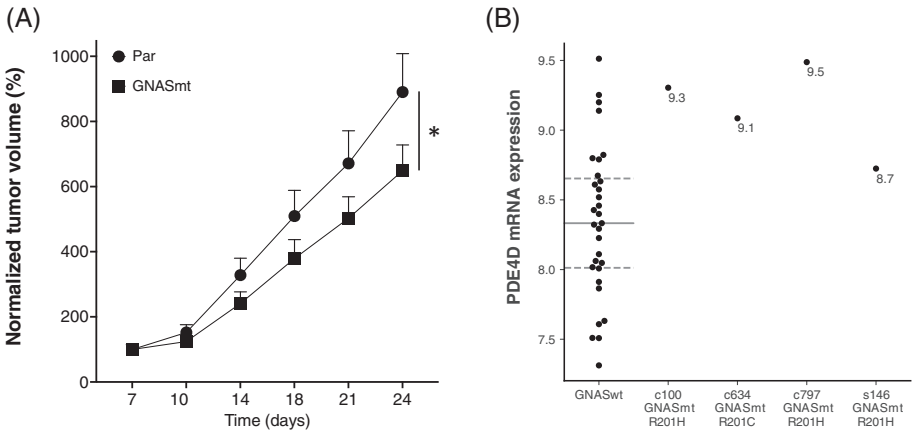

3.4 | GNASmt HCT116 cells form smaller tumors than the Par cells in mouse xenografts

In line with the in vitro findings, GNASmt HCT116 cell-derived tumors were smaller than those of Par cells, when grown subcutaneously in nude mice (Figure 4A). Additionally, the percentage of Ki67 immunopositive cells was significantly lower in the GNASmt tumors as compared to the Par tumors (93.6% ± 0.5% vs 95.6% ± 0.5%, $P = .02$). However, cleaved caspase 3 immunostaining revealed slightly more positivity in the Par tumors than in the GNASmt tumors (3.6% ± 0.3% vs 2.5% ± 0.2%, $P = .01$).

3.5 | *GNAS*-mutated human CRC tumors show high expression of *PDE4D*

To further validate the relationship between *GNAS* mutation and *PDE4D* expression, we analyzed *PDE4D* mRNA expression in *GNAS*

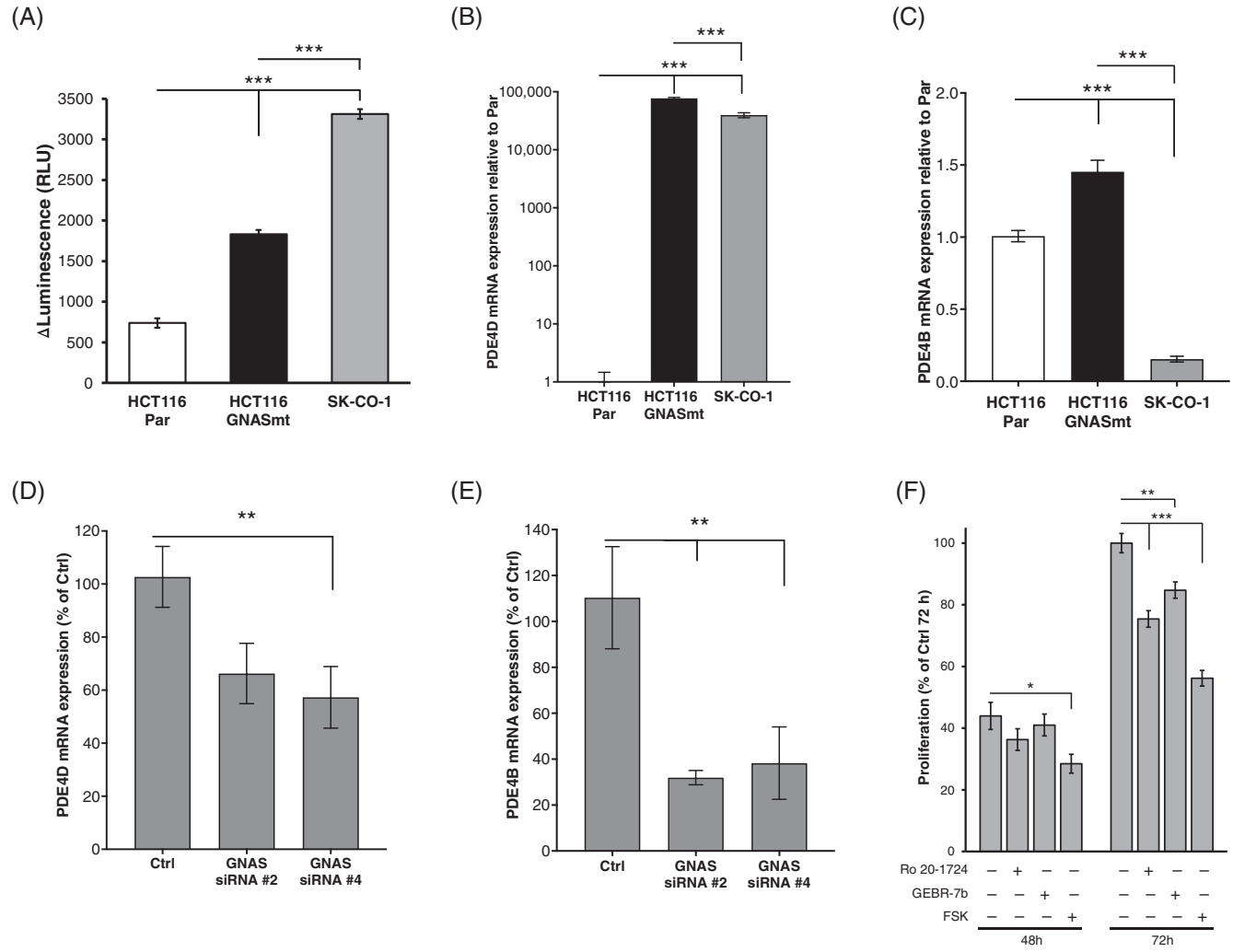

FIGURE 5 cAMP synthesis, expression of *PDE4D* and *PDE4B* transcripts, and proliferation of *GNAS*-mutated SK-CO-1 CRC cell line. (A) cAMP accumulation in Par and GNASmt HCT116 cells and in SK-CO-1 cells as measured with cAMP Glo Max assay. (B) Expression of *PDE4D* mRNA in Par and GNASmt HCT116 cells and in SK-CO-1 cells as analyzed with qPCR. (C) Expression of *PDE4B* mRNA in Par and GNASmt HCT116 cells and in SK-CO-1 cells as analyzed with qPCR. (D) Expression of *PDE4D* mRNA in SK-CO-1 cells after treatment with *GNAS* siRNAs. (E) Expression of *PDE4B* mRNA in SK-CO-1 cells after treatment with *GNAS* siRNAs. Scrambled siRNA was used as a control (Ctrl) in D and E. (F) Proliferation of SK-CO-1 cells with and without PDE4 inhibitors (Ro 20-1724, 10 μM and GEBR-7b, 10 μg/mL) or FSK (10 μM) as analyzed with CellTiter Blue Cell Viability Assay. The values are means ± SEM from three independent experiments, except two in A (n = 12 in A, n = 9 in B-E, n = 18 in F). * $P < .05$, ** $P < .01$, *** $P < .001$.

wild-type and mutant human CRC tumors. We identified four cases with *GNAS* codon 201 mutation (three R201H and one R201C) in a series of 35 CRCs, and all *GNAS* mutant tumors (n = 4) showed a high expression of *PDE4D* (Figure 4B). The median value of *PDE4D* expression for *GNAS* wild-type tumors (n = 31) was 8.33 (interquartile range, IQR 8.01-8.65), and *PDE4D* expression of all *GNAS* mutant tumors (n = 4) were in the fourth quartile of the wild-type tumors. Overall, *PDE4D* mRNA expression was upregulated in *GNAS* mutant tumors as compared to wild-type ones (FC = 1.8, $P = .014$). Further, three of the four *GNAS* mutant tumors showed moderate to strong immunostaining for PDE4D in the neoplastic cells (Figure S5). In addition to *PDE4D* mRNA, *PDE4B* mRNA expression showed higher values in *GNAS* mutant tumors, but the difference between them and *GNAS* wild-type tumors was not statistically significant (FC = 2.3, $P = .05$) (Figure S6). All four *GNAS* mutant tumors also contained a RAS pathway mutation (*BRAF* V600E in two, *KRAS* G13D in one and *KRAS* A146V in one), and two of them contained *APC* frameshift mutation. The four *GNAS* wild-type tumors showing the highest *PDE4D* expression did not contain *PRKACA* or *PRKAR1A* mutations, or *GNAS* or *PDE4D* gene fusions. Three of them contained *KRAS* codon 12 mutation (G12D, G12S and G12C) and one contained *NRAS* codon 12 mutation (G12V). None of the analyzed 35 CRC tumors contained mutations in the coding regions of *PDE4D* or *PDE4B* genes. Interestingly, both *PDE4D* and *PDE4B* expression showed a positive correlation with cyclooxygenase 2 (COX-2) gene (*PTGS2*, ENSG00000073756) expression in *GNAS* wild-type tumors (Pearson correlation $r = .52$, $P = .003$ for *PDE4D* and $r = .50$, $P = .004$ for *PDE4B*, n = 31 in both). GPCR activation due to COX-2 produced prostaglandin E_2 (PGE_2) might thus explain

the high *PDE4D/B* expression seen in some of the *GNAS* wild-type tumors.

3.6 | *GNAS* mutant SK-CO-1 CRC cell line is sensitive to PDE4 inhibition

To verify our findings in a CRC cell line intrinsically having an activating *GNAS* mutation, we utilized *GNAS* R201C mutated SK-CO-1 cell line. SK-CO-1 cells showed a high cAMP synthesis rate and a high *PDE4D* expression level (Figure 5A,B). *PDE4B* expression level, in turn, was low in SK-CO-1 cells (Figure 5C). Similarly to GNASmt HCT116 cells, *PDE4D* expression in SK-CO-1 cells was downregulated by *GNAS* siRNAs (Figure 5D). In contrast to GNASmt HCT116 cells, in this cell line also *PDE4B* expression was downregulated by *GNAS* silencing (Figure 5E). The effect of *GNAS* siRNAs on *GNAS* mRNA expression is shown in Figure S1B. Importantly, PDE4 inhibition or FSK inhibited the proliferation of SK-CO-1 cells (Figure 5F). PDE4 inhibitors did not induce apoptosis in these cells, but FSK induced a 2-fold increase in caspase 3/7 activity (Figure S4B). As a positive control, 1 μM staurosporine induced over 6-fold caspase activation (data not shown). SK-CO-1 cell line did not grow in the nude mouse model (<300 mm^3 tumors in 42 days after inoculating 4×10^6 cells in Matrigel; data not shown).

4 | DISCUSSION

We investigated the molecular and functional effects of mutated *GNAS* oncogene in CRC cell lines. Synthesis of cAMP was highly stimulated in GNASmt HCT116 cells as compared to the *GNAS* wild-type Par cells, which is in line with a previous publication using HT-29 CRC cells.[19] The topmost gene expression change induced by the *GNAS* mutation was a striking several hundred-fold induction of the cAMP-cleaving *phosphodiesterase PDE4D*. In contrast to *PDE4D*, which was expressed at a very low level in the Par HCT116 cells, *PDE4B* was highly expressed in the Par cells, which is consistent with earlier reports.[20,21] However, we show that expression of *PDE4B* was only slightly induced in the *GNAS*-mutated cells. Further, in the inherently *GNAS*-mutated SK-CO-1 cell line, showing even higher cAMP synthesis than the GNASmt HCT116 cells, the expression of *PDE4D* was high and that of *PDE4B* low. We also show that knockdown of *GNAS* downregulated expression of *PDE4D* in GNASmt HCT116 and SK-CO-1 cells, which indicates that activation of *GNAS* is the key regulator of *PDE4D* expression in these cells. The likely mechanism for *PDE4D* overexpression in *GNAS* mutant cells is the increase in cAMP production that leads to activation of PKA and CREB-mediated stimulation of cAMP response element (CRE) in the *PDE4D* gene promoter.[16,22] cAMP-induced *PDE4D* expression thus constitutes a compensatory mechanism to counteract the prolonged stimulation of cAMP synthesis caused by activating *GNAS* mutation. To support this, we obtained effective downregulation of *PDE4D* expression by PKA and CREB inhibitors, whereas an EPAC inhibitor was less effective. Finally, we demonstrated a high expression of *PDE4D* transcript and protein in *GNAS*-mutated human CRC tumor specimens as compared to *GNAS* wild-type ones, which indicates an important association between mutational activation of *GNAS* and *PDE4D* expression in human tumors as well. This is also supported by results published by Arang and Gutkind (n = 10,437),[2] who showed a higher than average prevalence of *GNAS* mutations (endometrial 7.4%, gastric 5.7%, pancreatic 5.0%, colon 4.5% and lung carcinoma 3.7%, as well as cutaneous melanoma 6.1%, vs pan-cancer average 2.3%) in cancer types reported to overexpress PDE4D.[11,12,14]

GNASmt HCT116 cells were less proliferative than the Par cells in vitro, and PDE4 inhibitors further suppressed the proliferation of GNASmt cells without an effect on the Par cells. The growth inhibitory effect of PDE4 inhibitors was also evident in the inherently *GNAS* mutant SK-CO-1 CRC cell line. Effect of PDE4 inhibitors on cell growth were demonstrated by both cell viability assay and thymidine incorporation assay. However, apoptosis was not induced by the PDE4 inhibitor Ro 20-1724, and negligible effect of another PDE4 inhibitor resveratrol on apoptosis has been demonstrated earlier in 2D cultures of HCT116 cells.[23] These data indicate that upregulation of PDE4D provides a growth advantage for *GNAS*-mutated CRC cells by modulating cAMP levels, and its pharmacologic inhibition leads to suppressed growth. As demonstrated by Li et al,[24] a potential mechanism for cAMP-induced growth suppression of HCT116 cells may depend on PKA-induced phosphorylation of BRAF and CRAF and a concomitant inhibition of ERK activation. In line with our results, CRISPR/Cas9-mediated *GNAS* R201H silencing has been shown to increase in vitro growth of a *GNAS*- and *KRAS*-mutated human pancreatic adenocarcinoma cell line.[25] Further, pharmacological inhibition of PDE4D or its gene silencing have been shown to suppress in vitro growth in multiple cancer cell lines, including breast, endometrial, gastric, hepatocellular, lung, ovarian and prostate carcinoma, as well as melanoma.[10,11,13]

More et al[26] have reported *GNAS* knockout to decrease in vitro colony formation and organoid growth of the inherently *GNAS* mutant CRC cell lines KM12, SNU175 and SK-CO-1. Furthermore, they reported that overexpression of either wild-type or mutant *GNAS* increased in vitro growth of LS174T CRC cells. One potential explanation for these opposite results on CRC cell growth after introduction of *GNAS* mutation is that More et al used a vector-based system utilizing tetracycline response element promoter, whereas we knocked in a gain-of-function mutation to the endogenous gene using CRISPR/Cas9 technology. These two distinct techniques may lead to different steady-state expression levels of the mutated protein, which could explain subsequent effects on cell growth. Further, More et al analyzed in vitro growth using colony formation assay, whereas we measured cell viability and thymidine incorporation. These assays measure distinct properties of 2D cell growth and survival. In vivo, More et al[26] have reported *GNAS* knockout to decrease the peritoneal growth of the *GNAS*-mutated CRC cell line KM12, and overexpression of wild-type or mutant *GNAS* to increase the growth of LS174T CRC cells. Our in vivo data show that Par HCT116 cells formed larger tumors than the *GNAS*-mutated ones in a subcutaneous nude mouse model. In line with our

results, *PDE4D* knockdown has been shown to reduce subcutaneous growth rate of prostate cancer cell lines.[10] One explanation for the discrepant results between peritoneal and subcutaneous in vivo models may depend on a different microenvironment.

GNAS and *KRAS* oncogenes are often co-mutated in tumors,[27,28] and both HCT116 and SK-CO-1 CRC cell lines are *KRAS*-mutated.[29] Previously, PDE4 inhibitors have been shown to require combination with FSK to decrease proliferation of *KRAS*-mutated and *GNAS* wild-type DLD1 and HCT116 CRC cells.[21,30] Similarly, PDE4 inhibition was not effective alone, but again required combination with FSK to inhibit proliferation of *GNAS* mutant and *KRAS*/*BRAF*V600 wild-type KM12C cells.[31] In our experiments, Par HCT116 cells did not respond to PDE4 inhibition alone, but in both the GNASmt HCT116 cells and the inherently *GNAS* mutant SK-CO-1 cells PDE4 inhibitors suppressed the cell growth as a single agent. To this end, it is interesting to note that half of the human *GNAS*-mutated CRC tumors in our series had a *KRAS* mutation. As the other half of these tumors contained *BRAF* V600E mutations, it is plausible to conclude that combination of *GNAS* and *RAS* or *BRAF* V600E mutations is necessary to increase cAMP to such levels that leads to overexpression of PDE4D. It is also interesting to note that CRC cell lines show enrichment of microsatellite instability (MSI) as compared to CRC tumors, and also HCT116 cell line is MSI.[29] However, the SK-CO-1 cell line is microsatellite stable, as were all *GNAS*-mutated human CRC tumor specimens in our series, indicating that the relationship between *GNAS* activation and *PDE4D* overexpression takes place in both microsatellite stable and unstable conditions.

The *PDE4D* gene gives rise to the highest number of transcript variants of the *PDE4* genes, and these variants differ markedly in their N-terminal regions.[8] PDE4D1-9 protein isoforms are enzymatically active, whereas PDE4DN1-3 are inactive due to the missing parts of catalytic domain (so-called dead-short variants). Of the enzymatically active isoforms, PDE4D1 is short, PDE4D2 and D6 are supershort, and the rest are long isoforms. Long isoforms can form dimers and they can be activated by PKA through phosphorylation,[32] which is an important negative regulation loop for cAMP signaling. ERK-mediated phosphorylation in turn inhibits the activity of most PDE4D isoforms, except the short isoform D1, which is conversely activated.[33] Interestingly, *GNAS* mutation induced the expression of short and supershort variants *PDE4D1*, *PDE4D2* and *PDE4D6* in the HCT116 cells. These variants are known to be transcriptionally upregulated by PKA activated CREB binding to the CRE in their promoter.[34] In several cell types, including Jurkat T-cells, NIH3T3 cells, and activated vascular smooth muscle cells, cAMP elevation has been found to specifically induce expression of the short and supershort variants *PDE4D1* and *PDE4D2*.[35,36] In addition, epigenetic regulation may also play a role, since histone acetylation of the intronic promoter regulating *PDE4D1* and *PDE4D2* expression was shown to allow selective cAMP-mediated induction of these transcript variants.[36] In our model, at least in HCT116 cells, it seems evident that of the PDE4D isoforms the short and supershort variants play the major role in regulation of cAMP levels and subsequent growth control of these cancer cells.

In conclusion, we show that activating *GNAS* mutation induces cAMP synthesis and results in growth suppression of CRC cells. Clearly, other cellular mechanisms beyond proliferation are responsible for *GNAS* gene's oncogenic potential. Importantly, our study underlines the importance of compensatory PDE4 upregulation to provide a growth advantage to *GNAS*-mutated CRC cells, and the pharmacological use of PDE4 inhibitors could potentially impede the growth of *GNAS*-mutated tumors.

AUTHOR CONTRIBUTIONS

The work reported in the article has been performed by the authors, unless clearly specified in the text. **Pirjo Nummela:** Conceptualization; investigation and data analysis; supervision; writing-original draft; writing-review and editing. **Sadia Zafar:** Conceptualization; investigation and data analysis; supervision; writing-original draft; writing-review and editing. **Erika Veikkolainen:** Investigation and data analysis; writing-review and editing. **Iiris Ukkola:** Investigation and data analysis; writing-review and editing. **Vincenzo Cinella:** Investigation and data analysis; writing-review and editing. **Abiodun Ayo:** Investigation and data analysis; writing-review and editing. **Muhammad Yasir Asghar:** Investigation and data analysis; writing-review and editing. **Niko Välimäki:** Investigation and data analysis; writing-review and editing. **Kid Törnquist:** Supervision; writing-review and editing. **Auli Karhu:** Supervision; writing-review and editing. **Pirjo Laakkonen:** Supervision; writing-review and editing. **Lauri A. Aaltonen:** Supervision; writing-review and editing. **Ari Ristimäki:** Conceptualization; supervision; writing-original draft; writing-review and editing.

ACKNOWLEDGMENTS

We thank M. Haukka, A. Schoonenberg and K. Räsänen for excellent technical assistance, and J. Väänänen for RNA-Seq data analysis service. We further thank the FIMM Digital Microscopy and Molecular Pathology Unit, and FIMM Genomics Unit (Helsinki Institute of Life Science HiLIFE, University of Helsinki) for immunohistochemical staining and cell line authentication services, respectively. Biomedicum Functional Genomics Unit (HiLIFE and Biocenter Finland, University of Helsinki) is acknowledged for RNA-Seq service.

FUNDING INFORMATION

This study was supported by the Cancer Foundation Finland, Finska Läkaresällskapet, Helsinki University Hospital Research Funds, Medicinska Understödsföreningen Liv och Hälsa, the Sigrid Jusélius Foundation and the University of Helsinki. The services of the FIMM Digital Microscopy and Molecular Pathology Unit, FIMM Genomics Unit and Biomedicum Functional Genomics Unit are supported by the University of Helsinki (HiLIFE) and Biocenter Finland.

CONFLICT OF INTEREST STATEMENT

The authors have no competing interests.

DATA AVAILABILITY STATEMENT

The raw RNA-Seq data generated in this study is available in GEO under accession number GSE231943 (https://www.ncbi.nlm.nih.gov/geo/query/acc.cgi?acc=GSE231943). Other data that support the

findings of this study are available from the corresponding author upon request.

ETHICS STATEMENT

The mice experiments were performed with the approval of the Committee for Animal Experiments of the District of Southern Finland (ESAVI/22896/2020, ESAVI/10262/2022). The study of human tumors has been reviewed and approved by the Ethics Committee of the Hospital District of Helsinki and Uusimaa (HUS/2509/2016) and the Finnish Institute for Health and Welfare (THL/1300/5.05.00/2019). All samples were collected after informed consent.

ORCID

Pirjo Nummela https://orcid.org/0000-0002-2768-8816
Sadia Zafar https://orcid.org/0000-0002-6340-1077
Erika Veikkolainen https://orcid.org/0009-0005-5610-0048
Iiris Ukkola https://orcid.org/0009-0002-7153-2648
Vincenzo Cinella https://orcid.org/0009-0002-8555-2906
Abiodun Ayo https://orcid.org/0000-0003-4173-162X
Muhammad Yasir Asghar https://orcid.org/0000-0002-1935-8462
Ari Ristimäki https://orcid.org/0000-0002-5373-9234

REFERENCES

1. Ramms DJ, Raimondi F, Arang N, Herberg FW, Taylor SS, Gutkind JS. Galphas-protein kinase A (PKA) pathway signalopathies: the emerging genetic landscape and therapeutic potential of human diseases driven by aberrant Galphas-PKA signaling. *Pharmacol Rev*. 2021;73:155-197.
2. Arang N, Gutkind JS. G protein-coupled receptors and heterotrimeric G proteins as cancer drivers. *FEBS Lett*. 2020;594:4201-4232.
3. Ahmed MB, Alghamdi AAA, Islam SU, Lee JS, Lee YS. cAMP signaling in cancer: a PKA-CREB and EPAC-centric approach. *Cell*. 2022;11:2020.
4. Afolabi HA, Salleh SM, Zakaria Z, et al. A GNAS gene mutation's independent expression in the growth of colorectal cancer: a systematic review and meta-analysis. *Cancers*. 2022;14:5480.
5. Domingo E, Camps C, Kaisaki PJ, et al. Mutation burden and other molecular markers of prognosis in colorectal cancer treated with curative intent: results from the QUASAR 2 clinical trial and an Australian community-based series. *Lancet Gastroenterol Hepatol*. 2018;3:635-643.
6. Hsien Lai S, Zervoudakis G, Chou J, Gurney ME, Quesnelle KM. PDE4 subtypes in cancer. *Oncogene*. 2020;39:3791-3802.
7. Omori K, Kotera J. Overview of PDEs and their regulation. *Circ Res*. 2007;100:309-327.
8. Paes D, Schepers M, Rombaut B, van den Hove D, Vanmierlo T, Prickaerts J. The molecular biology of phosphodiesterase 4 enzymes as pharmacological targets: an interplay of isoforms, conformational states, and inhibitors. *Pharmacol Rev*. 2021;73:1016-1049.
9. Mehta A, Patel BM. Therapeutic opportunities in colon cancer: focus on phosphodiesterase inhibitors. *Life Sci*. 2019;230:150-161.
10. Rahrmann EP, Collier LS, Knutson TP, et al. Identification of PDE4D as a proliferation promoting factor in prostate cancer using a sleeping beauty transposon-based somatic mutagenesis screen. *Cancer Res*. 2009;69:4388-4397.
11. Lin DC, Xu L, Ding LW, et al. Genomic and functional characterizations of phosphodiesterase subtype 4D in human cancers. *Proc Natl Acad Sci U S A*. 2013;110:6109-6114.
12. Liu F, Ma J, Wang K, et al. High expression of PDE4D correlates with poor prognosis and clinical progression in pancreatic ductal adenocarcinoma. *J Cancer*. 2019;10:6252-6260.
13. Ragusa F, Panera N, Cardarelli S, et al. Phosphodiesterase 4D depletion/inhibition exerts anti-oncogenic properties in hepatocellular carcinoma. *Cancers*. 2021;13:2182.
14. Cao B, Wang K, Liao JM, et al. Inactivation of oncogenic cAMP-specific phosphodiesterase 4D by miR-139-5p in response to p53 activation. *Elife*. 2016;5:e15978.
15. Saarinen L, Nummela P, Leinonen H, et al. Glycomic profiling highlights increased fucosylation in pseudomyxoma peritonei. *Mol Cell Proteomics*. 2018;17:2107-2118.
16. Wang D, Deng C, Bugaj-Gaweda B, et al. Cloning and characterization of novel PDE4D isoforms PDE4D6 and PDE4D7. *Cell Signal*. 2003;15:883-891.
17. Cajuso T, Sulo P, Tanskanen T, et al. Retrotransposon insertions can initiate colorectal cancer and are associated with poor survival. *Nat Commun*. 2019;10:4022.
18. Katainen R, Donner I, Cajuso T, et al. Discovery of potential causative mutations in human coding and noncoding genome with the interactive software BasePlayer. *Nat Protoc*. 2018;13:2580-2600.
19. Nishikawa G, Sekine S, Ogawa R, et al. Frequent GNAS mutations in low-grade appendiceal mucinous neoplasms. *Br J Cancer*. 2013;108:951-958.
20. Tsunoda T, Ota T, Fujimoto T, et al. Inhibition of phosphodiesterase-4 (PDE4) activity triggers luminal apoptosis and AKT dephosphorylation in a 3-D colonic-crypt model. *Mol Cancer*. 2012;11:46.
21. Kim DU, Kwak B, Kim SW. Phosphodiesterase 4B is an effective therapeutic target in colorectal cancer. *Biochem Biophys Res Commun*. 2019;508:825-831.
22. Le Jeune IR, Shepherd M, van Heeke G, Houslay MD, Hall IP. Cyclic AMP-dependent transcriptional up-regulation of phosphodiesterase 4D5 in human airway smooth muscle cells. Identification and characterization of a novel PDE4D5 promoter. *J Biol Chem*. 2002;277:35980-35989.
23. Tsunoda T, Ishikura S, Doi K, Matsuzaki H, Iwaihara Y, Shirasawa S. Resveratrol induces luminal apoptosis of human colorectal cancer HCT116 cells in three-dimensional culture. *Anticancer Res*. 2014;34:4551-4555.
24. Li Y, Takahashi M, Stork PJS. Ras-mutant cancer cells display B-Raf binding to Ras that activates extracellular signal-regulated kinase and is inhibited by protein kinase A phosphorylation. *J Biol Chem*. 2013;288:27646-27657.
25. Kawabata H, Ono Y, Tamamura N, et al. Mutant GNAS limits tumor aggressiveness in established pancreatic cancer via antagonizing the KRAS-pathway. *J Gastroenterol*. 2022;57:208-220.
26. More A, Ito I, Haridas V, et al. Oncogene addiction to GNAS in GNAS(R201) mutant tumors. *Oncogene*. 2022;41:4159-4168.
27. Nummela P, Saarinen L, Thiel A, et al. Genomic profile of pseudomyxoma peritonei analyzed using next-generation sequencing and immunohistochemistry. *Int J Cancer*. 2015;136:E282-E289.
28. Tirosh A, Jin DX, de Marco L, Laitman Y, Friedman E. Activating genomic alterations in the Gs alpha gene (GNAS) in 274 694 tumors. *Genes Chromosomes Cancer*. 2020;59:503-516.
29. Mouradov D, Sloggett C, Jorissen RN, et al. Colorectal cancer cell lines are representative models of the main molecular subtypes of primary cancer. *Cancer Res*. 2014;74:3238-3247.
30. Kim DU, Nam J, Cha MD, Kim SW. Inhibition of phosphodiesterase 4D decreases the malignant properties of DLD-1 colorectal cancer cells by repressing the AKT/mTOR/Myc signaling pathway. *Oncol Lett*. 2019;17:3589-3598.
31. McEwan DG, Brunton VG, Baillie GS, Leslie NR, Houslay MD, Frame MC. Chemoresistant KM12C colon cancer cells are addicted to low cyclic AMP levels in a phosphodiesterase 4-regulated

compartment via effects on phosphoinositide 3-kinase. *Cancer Res*. 2007;67:5248-5257.
32. Xie M, Blackman B, Scheitrum C, et al. The upstream conserved regions (UCRs) mediate homo- and hetero-oligomerization of type 4 cyclic nucleotide phosphodiesterases (PDE4s). *Biochem J*. 2014; 459:539-550.
33. MacKenzie SJ, Baillie GS, McPhee I, Bolger GB, Houslay MD. ERK2 mitogen-activated protein kinase binding, phosphorylation, and regulation of the PDE4D cAMP-specific phosphodiesterases. The involvement of COOH-terminal docking sites and NH2-terminal UCR regions. *J Biol Chem*. 2000;275:16609-16617.
34. Kyurkchieva E, Baillie GS. Short PDE4 isoforms as drug targets in disease. *Front Biosci*. 2023;28:133.
35. Erdogan S, Houslay MD. Challenge of human Jurkat T-cells with the adenylate cyclase activator forskolin elicits major changes in cAMP phosphodiesterase (PDE) expression by up-regulating PDE3 and inducing PDE4D1 and PDE4D2 splice variants as well as down-regulating a novel PDE4A splice variant. *Biochem J*. 1997;321:165-175.
36. Tilley DG, Maurice DH. Vascular smooth muscle cell phenotype-dependent phosphodiesterase 4D short form expression: role of differential histone acetylation on cAMP-regulated function. *Mol Pharmacol*. 2005;68:596-605.

SUPPORTING INFORMATION

Additional supporting information can be found online in the Supporting Information section at the end of this article.

How to cite this article: Nummela P, Zafar S, Veikkolainen E, et al. *GNAS* mutation inhibits growth and induces phosphodiesterase 4D expression in colorectal cancer cell lines. *Int J Cancer*. 2024;154(11):1987-1998. doi:10.1002/ijc.34865